ACS APPLIED MATERIALS & INTERFACES

Research Article

www.acsami.org

Preparation of Boron-Doped Porous Titania Networks Containing Gold Nanoparticles with Enhanced Visible-Light Photocatalytic Activity

Xingdong Wang,[†,‡] Mark Blackford,[§] Kathryn Prince,[§] and Rachel A. Caruso*[,†,‡]

[†]CSIRO Materials Science and Engineering, Clayton, Victoria 3168 (Australia)

[‡]PFPC, School of Chemistry, The University of Melbourne, Melbourne, Victoria 3010 (Australia)

[§]Australian Nuclear Science and Technology Organisation, PMB 1, Menai, NSW 2234 (Australia)

Supporting Information

ABSTRACT: The ability to decrease the electron/hole recombination rate, and decrease the band gap of titania to allow photoactivity on irradiation with visible light is attracting more and more attention. Here, boron doping of the titania, the deposition of gold nanoparticles, along with a meso-macroporous structure were obtained using a facile agarose gel templating process combined with sol−gel chemistry. The Au/B/TiO_2 nanocomposites were characterized using SEM, TEM, XRD, N_2 gas sorption, diffuse UV−vis, photoluminescence, and SIMS. The photocatalytic activity was assessed by degradation of an organic probe molecule (methylene blue) under visible light (λ > 420 nm). The resulting materials achieved photocatalytic activities up to 50% greater than the commercial Degussa P25 under visible light. The enhancement in photocatalytic activity was primarily attributed to the decrease in band gap as a result of the boron doping and its influence on the anatase to rutile phase formation: The doped materials were highly crystalline and an optimum anatase to rutile ratio (3:1) was obtained with 0.25 wt % boron in the sample calcined at 650 °C. In addition, the presence of the gold nanoparticles decreased recombination between the photoexcited electrons and holes, which further improved the photocatalytic activity.

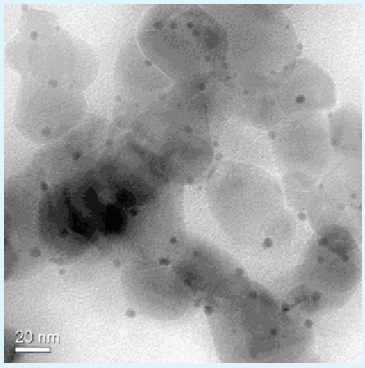

KEYWORDS: *gold nanoparticles, titania, boron doping, photocatalysis, visible light*

INTRODUCTION

The titania (TiO_2)-based photocatalysts have promising applications in environmental remediation for the photocatalytic decomposition of organic pollutants. Among the three natural crystalline phases (anatase, rutile and brookite) of titania, the anatase and rutile phases have been extensively studied for their photocatalytic (PC) activity. It is commonly believed that the anatase phase has the greatest PC activity in UV light (λ < 400 nm, only 5% of sunlight).[1,2] However, in terms of environmental cleanup utilizing natural solar light (primarily visible light with photons of λ > 400 nm), the wider band gap (3.2 eV, λ < 387 nm) of the anatase phase (compared to the slightly narrower band gap, 3.0 eV, of the rutile phase), make it relatively inactive.[3] Moreover, TiO_2 has other limitations, chiefly, the high recombination rate of photoexcited electrons and holes (~90% undergo recombination),[4] and the interactions between the organic pollutant and the active sites on the surface of nonporous titania being limited due to the low surface/volume ratio,[1,2] which acts to further restrict its PC activity.[3]

One of the common approaches to increase the response of TiO_2 to visible light, is doping of a foreign element into the titania crystal lattice, which can decrease the band gap to below the threshold energy (<3.0 eV) of visible light absorption (λ > 400 nm).[5] The elements most often used to dope the TiO_2 include transition metal ions (e.g., Fe, W, and Cr) and nonmetallic atoms (e.g., C, N, S, F, and I).[6,7] Recently, boron has emerged as a nonmetallic dopant that enhances visible light response. However, some controversial results were reported as the preparation method plays an important role in determining the properties of the materials, and hence their activity, such as optimum level of boron doping, oxidation state, position of B in the anatase crystal and the doping process itself.[8−13] It was found that boron doping can improve the visible-light absorption significantly, though it does not always result in significant visible light photocatalytic activity. This may be caused by the promotion of structural defects with doping (e.g., formation of Ti^{3+}) that lead to charge recombination.[12,14] Research has been undertaken to further improve the visible light activity of boron doped samples by codoping with another element, such as Ni, N, S, and C.[8,12,13,15−17] The codoping was used to facilitate the separation and transfer of the charge carriers.[13] It is well-documented that gold nanoparticles effectively increase charge separation as the noble metal nanoparticles serve as electron sinks, thus decreasing the recombination of photoexcited electron/hole pairs, thereby

Received: December 1, 2011
Accepted: December 23, 2011
Published: January 13, 2012

improving the PC activity of the titania materials.[4,18−24] However, there is no report to date on boron doping coupled with Au nanoparticle deposition to improve the charge separation and thereby enhance the PC activity of titania in the visible light range. In this contribution, gold nanoparticles were added to increase the charge separation within B/TiO_2. The combination of these approaches intergrates the advantages of the individual systems to enhance the PC activity of TiO_2. Specifically, boron was doped in the titania crystal to decrease the band gap, gold nanoparticles were incorporated in the structure as they act as an electron sink in the materials thereby decreasing electron/hole recombinations, and a highly porous, nanoparticulate network was fabricated with substantial surface area. The Au/B/TiO_2 composites, with a range of B/TiO_2 contents (ratio of 0−4 wt %, calculated from the quantities used during synthesis) and 2 wt % Au, were prepared by using a simple agarose gel templating technique. The gold content chosen had resulted in the highest PC activity under UV light for Au/TiO_2 samples.[25] Also studied was the effect of calcination temperature (450 and 650 °C) when fabricating the B/TiO_2 composites on the PC activity under visible light.

EXPERIMENTAL SECTION

Preparation of Porous Au/B/TiO_2 Nanomaterials. The agarose templating technique was adapted to form the porous structure in the Au/B/TiO_2 composites. As mentioned in our previous publication,[25] there are five basic steps used to fabricate the pure porous TiO_2 composites using the agarose templating technique. Briefly, 100 g of 2 wt % agarose gel template was formed by cooling a boiled aqueous solution containing dissolved agarose powder (2 g, Scientifix (molecular biology grade)) overnight in a test tube. The gel was removed from the glass test tube and cut into small pieces (approximate size of 0.5 × 0.5 × 0.5 cm^3). After solvent exchange from water to isopropanol, the gel (6 g for each solution) was placed in a mixture (22 mL) of 0, 0.1, 0.2, 0.4, 0.8, or 1.6 mL of a 2.313 M H_3BO_3 in methanol solution and 70 wt % titanium precursor (titanium(IV) isopropoxide (97%)) in isopropanol, with the aim of achieving a uniform B-doping throughout the porous titania matrix. After hydrolysis and condensation reactions were conducted by soaking these infiltrated agarose gel pieces in a water/isopropanol (1:1 volume, 22 mL) solution, the samples were then removed from the solution and dried at room temperature in a fumehood for 2 days followed by 6 h at 60 °C. The samples were calcined with a ramp of 3.54 °C min^{-1} to 450 or 650 °C for 10 h under flowing air. This led to the formation of boron doped TiO_2 composites with a variation in B content (0−4 wt % calculated from the quantities used during synthesis). Au deposition onto the preformed B/TiO_2 porous structures was conducted using a deposition precipitation procedure.[25] The quantity (2 wt % referring to Au mass/TiO_2 mass) and conditions of gold deposition (pH 7) were chosen as they were shown to give the highest PC activity under UV light.[25] The B/TiO_2 networks (1 g) were placed overnight in the gold precursor solutions ($HAuCl_4$ solution: 100 mM, 1 mL) with pH preadjusted to 7 using a 0.017 M $NaCO_3$ solution, and then heated at 70 °C for 3 h. The samples were washed thoroughly to remove the chloride, dried and then calcined at 300 °C (ramp rate of 3.54 °C/min) for 5 h to obtain a strong Au attachment to the surface of titania.

Characterization of the Materials. Transmission electron microscopy (TEM) and Scanning Transmission electron microscopy (STEM) images were taken using either a Philips CM120 BioTWIN TEM operating at 120 kV or a JEOL 2010F TEM operating at 200 kV, fitted with a Gatan Imaging Filter (GIF) and an Oxford Instruments ISIS energy-dispersive X-ray spectroscopy (EDS) system, for qualitative analysis. The samples were embedded in an LR-white resin and ultramicrotomed to a thickness of 90 nm before TEM analysis. Scanning electron microscopy (SEM, Philips XL30 FEGSEM or FEI QUANTA 200F, operated at 20 kV) was used to examine the morphology of the samples.

Nitrogen gas sorption measurements were conducted on a Micromeritics 3000 Tristar surface area and porosity analyzer at 77 K. Samples were evacuated at 150 °C overnight before analysis. Surface areas were calculated by using the Brunauer−Emmett−Teller (BET) method. X-ray diffraction (XRD) was performed using a Philips PW1800 diffractometer (CuKα radiation wavelength of 1.54045 Å) to characterize the phase and crystal size of the final product.

UV−visible diffuse reflecting spectra of the Au/B/TiO_2 composites were recorded on a Cary 5G UV−vis−IR spectrophotometer. Photoluminescence (PL) measurements of the Au/B/TiO_2 composites were carried out on a Perkin-Elmer Luminescence spectrometer LS 50. The emission and excitation wavelength was 420 and 260 nm respectively, using a cutoff filter of 290 nm.

Thermogravimetric analysis (TGA) and differential thermal analysis (DTA) were performed on a Mettler Toledo TGA/SDTA851e analyzer. The weight loss of organic and the amorphous to anatase phase transition temperature of the TiO_2 were studied by TGA and DTA. The samples were stabilized at 25 °C for 5 min before they were heated from 25 to 800 °C with a heating rate of 10 °C/min, under oxygen (30 mL/min).

The distribution of the gold in the porous titania was investigated using a Camera IMS 5f dynamic secondary ion mass spectrometer (SIMS). The samples were mounted into EPO-THIN epoxy resin (Selby-Biolab), and polished carefully to achieve a smooth surface. The surface of the samples was sputter coated with carbon to minimize charging during SIMS analysis. A 10 keV Cs^+ primary ion source was used to generate negative secondary ions (^{18}O, ^{49}Ti, $^{49}Ti^{18}O$, $^{49}Ti^{16}O$,$^{49}Ti^{16}O_2$, $^{49}Ti^{18}O_2$, ^{197}Au, and ^{11}B) which were counted for 1 s each per cycle on an ETP electron multiplier. A 60 nA primary ion beam, with an approximate diameter of ∼50 μm, was rastered over each sample surface creating a crater with approximate dimensions of 250 × 250 μm^2. An aperture in the secondary column was used to provide an analytical area of diameter 55 μm in all measurements, thereby minimizing any crater edge effects in the analysis. Each sample surface was sputtered for around 1000 s prior to analysis to enable equilibrium sputtering conditions to be achieved. Further Cs^+ bombardment for 2000 s allowed stable counts for each mass channel of interest to be collected. The resulting craters were around 5 μm deep. Crater depth was determined using a KLA Tencor Alpha-step IQ stylus profilometer.

Photocatalytic Activity Measurements. The photocatalytic activity was evaluated through the decomposition of methylene blue under visible light irradiation. Light with a wavelength range of 420 - 650 nm was reflected from a dichroic mirror. The amount of photocatalyst used was 1.0 g L^{-1}, and the methylene blue concentration was 12.5 ppm. During the photocatalytic reaction, the concentration of methylene blue was monitored by observing the solution absorbance at 664 nm using a UV−vis spectrometer (CARY50 Bio UV−visible spectrophotometer) every 30 min for 2 h.

The photocatalytic activity, given as a percentage, refers to the difference in methylene blue concentration immediately before irradiation, $C(0)$, and after 120 min of visible light irradiation, $C(120)$, divided by the concentration before irradiation (i.e., $100[C(0) - C(120)]/C(0)$).

RESULTS AND DISCUSSION

Materials Preparation. Here, we report a simple synthesis method that combines boron doping and gold nanoparticle incorporation within porous TiO_2 structures. The porous Au/B/TiO_2 materials were prepared by adopting a facile agarose gel templating technique, which has been well-established for the production of nondoped porous metal oxide materials (such as TiO_2 or ZrO_2).[26] Briefly, the porous agarose gel template was formed after cooling the boiled agarose aqueous solution. The precursors of boron and titania were mixed at various ratios (B/

dx.doi.org/10.1021/am201695c | ACS Appl. Mater. Interfaces 2012, 4, 476−482

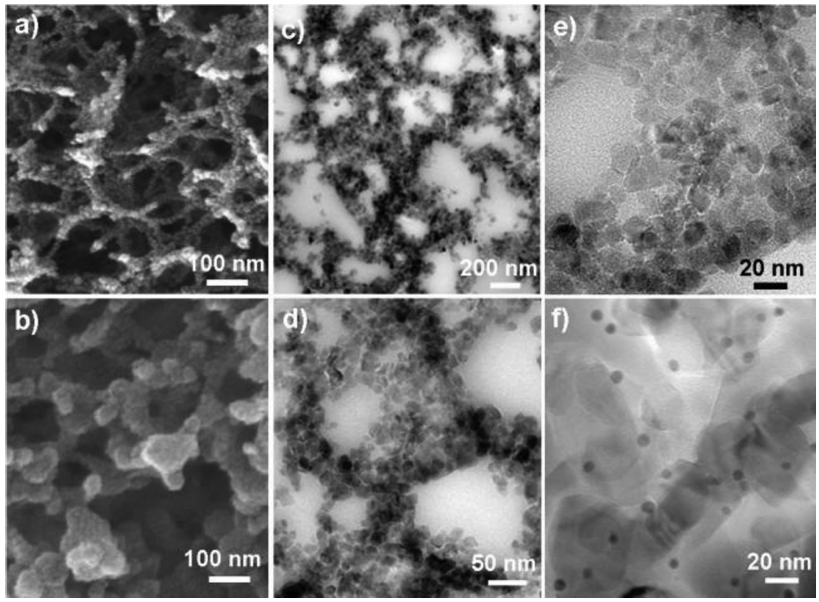

Figure 1. (a, b) SEM and (c–f) TEM images of the Au/B/TiO_2 composites with initial boron and Au contents of 0.25 and 2 wt %, respectively. The calcination temperature was (a) 450 °C and (b–f) 650 °C. The magnification increases from c–e using traditional TEM mode, whereas f is a high magnification using plasmon mode to emphasize the gold nanoparticles.

TiO_2 wt %: 0, 0.25, 0.5, 1.0, 2.0, and 4.0) and infiltrated into the agarose template. After the hydrolysis and condensation reactions, calcination (450 or 650 °C for 10 h) was conducted to remove the agarose and crystallize the B/TiO_2 materials. The two calcination temperatures and the boron doping quantities were changed to examine the effect this had on the crystal properties, such as crystal size and the crystal phase ratio between anatase and rutile. Finally, gold nanoparticles were added to these porous matrices using a modified deposition precipitation method at pH 7.[25]

Characterization of Au/B/TiO_2. The calcined materials have interconnected pore structures throughout the network (Figure 1). An increase in boron content barely influenced the average pore size, slightly increased the wall thickness, and slightly decreased the diameter of the TiO_2 particles (discussed later). In contrast, increasing calcination temperature dramatically decreased the average pore size (150 nm calcined at 450 °C compared with 70 nm calcined at 650 °C). The decreased pore size was probably caused by the significant increase in wall thickness when the sample was calcined at the higher temperature (compare Figure 1a and 1b). The average particle diameter of the TiO_2 nanoparticles composing the wall increased from ca. 20 nm (450 °C) to 30–40 nm (650 °C).

The highly porous structure of the Au/B/TiO_2 composites can also be observed in Figures 1c and d. The pores are indicated by the brighter areas in the traditional TEM mode images. Plasmon mode images, see Figure 1f for an example, were beneficial to locate the gold nanoparticles. The average gold particle size was around 2–5 nm in all of the samples; the boron content or the titania phase had negligible influence on this size.

The pore size distribution, see Figure S1 in the Supporting Information, was calculated by the Barrett, Joyner, Halenda (BJH) method using the desorption branch. The porous networks showed a dual pore size distribution, with macropores centered at 50 ± 10 or 55 ± 10 nm, and mesopores centered at 5 ± 2 or 24 ± 10 nm for the materials calcined at 450 and 650 °C, respectively. The macropores are a result of the use of the agarose gel template.[27] The small mesopores are due to the interparticle spacing, whereas the large mesopore could be template induced, resulting from coating of the agarose fibers, as opposed to the macropores already in the agarose structure.

The surface areas of the samples were significantly higher when calcined at the lower temperature (i.e., 450 °C) at the same initial boron content, and increased with an increase in the boron content during synthesis at the same calcination temperature (Figure 2). This is due to a smaller TiO_2 crystal size being obtained for the lower calcination temperature and higher boron doping as evidenced in the XRD data (see Figure 3 and Table S1 in the Supporting Information).

The samples were exclusively anatase when they were calcined at 450 °C (Figure 3a). The introduction of boron retarded the anatase crystal growth resulting in lower crystallinity. This is evidenced by broadening of the anatase peaks and decreasing of the peak intensity accordingly.[28] The crystal size decreased from 14 ± 1 nm for nondoped TiO_2 to 11 ± 1 nm for the 4 wt % boron sample, as calculated using the Scherrer equation and the (111) anatase peak.

When the calcination temperature increased to 650 °C, both anatase and rutile phases existed (Figure 3b). The crystal size of the anatase in the 650 °C calcined materials decreased from 32 ± 1 nm for nondoped titania to 29 ± 1 nm for 4 wt % boron. Boron doping remarkably suppressed the formation of the rutile phase (even with very low boron content, 0.25 wt %, indicated by the absence of several rutile peaks) as the peak intensity from the rutile phase decreased with an increase in the boron content. This retardation of the phase transition from anatase to rutile has been observed with other nonmetal or metal dopants.[29,30] The molar ratio of the anatase (or rutile) phase relative to the total crystalline sample was calculated using the following equations:

$$X_A = 1/(1 + 1.265 I_R/I_A);\ X_R = 1 - X_A$$

where X_A and X_R are the molar fractions of anatase and rutile, respectively, I_A denotes the intensity of the strongest anatase reflection (here, A_{101}, $2\theta = 25.4 \pm 0.1°$), and I_R is the intensity

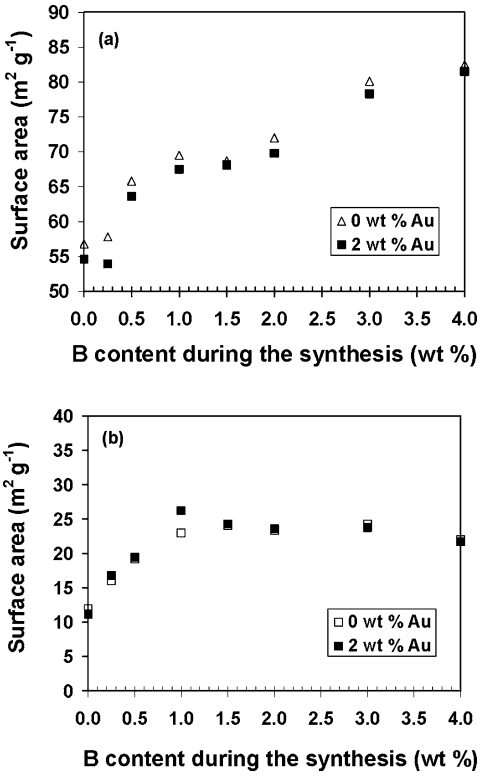

Figure 2. Surface area of the B/TiO_2 composites containing 0 or 2 wt % gold for various boron contents during synthesis. The samples were calcined at a temperature of (a) 450 °C or (b) 650 °C (The error associated with gas sorption analysis was less than 3% for these samples).

of the strongest rutile reflection (here, R_{110}, $2\theta = 27.7 \pm 0.1°$), according to Spurr and Myers' method.[31] For a given sample, the ratio I_A/I_R is independent of fluctuations in diffractometer characteristics. The X_A increased gradually from 0.60 for nondoped titania to 0.93 with 1.0 wt % boron, and then remained constant up to 4 wt % boron (see Table S1 in the Supporting Information). It is worth noting that the X_A of the sample with 0.25 wt % boron content (0.76) was very close to that of the commercial Degussa P25 titania (X_A of 0.78).

The gold deposition had no influence on the titania phase composition and intensity, as indicated by the similarity in the XRD pattern of 0 wt % of gold in the nondoped titania (0B0Au) and 2 wt % of gold in the nondoped titania (0), Figure 3b. A gold peak could not be detected by XRD because of the uniform distribution of the small gold clusters in the TiO_2 matrix and the relatively low gold content (2 wt %).[25]

Differential thermal analysis (DTA) was used to further study the influence of boron on the phase transition of the porous titania materials. An endothermic peak occurred around 80−100 °C and can be ascribed to the evaporation of water or organic solvent (e.g., isopropanol) from the materials (Figure 4). The exothermic peak at ca. 240−260 °C was caused by the thermal degradation of the agarose gel template. The exothermic peak which appeared around 400−450 °C was ascribed to the phase transition from the amorphous to the anatase crystal phase. The phase transition temperature increased as the boron content increased, from 402 °C for the nondoped sample to 445 °C for the 4 wt % boron sample. No obvious exothermic peak appeared at around 650 °C to indicate transition to the rutile phase. This is reasonable as there was only partial transformation to the rutile phase and less energy is required in the anatase to rutile phase transition compared with the amorphous to anatase phase transition.[32]

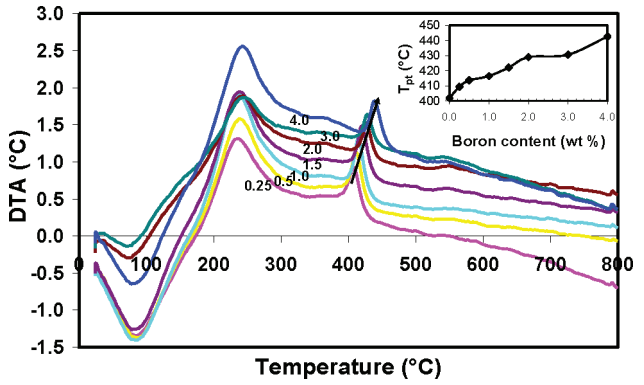

Figure 4. DTA data of B/TiO_2 composites with 0.25−4 wt % boron during synthesis, and inset the phase transition temperature (T_{pt}, taken as the temperature corresponding to the exothermic peak above 400 °C) as a function of the boron content during synthesis.

From SIMS studies, the yields of both gold (^{197}Au) and boron (^{11}B) secondary ions were observed to be relatively uniformly distributed through the porous titania network over 5 μm in depth. The boron content gradually increased as the

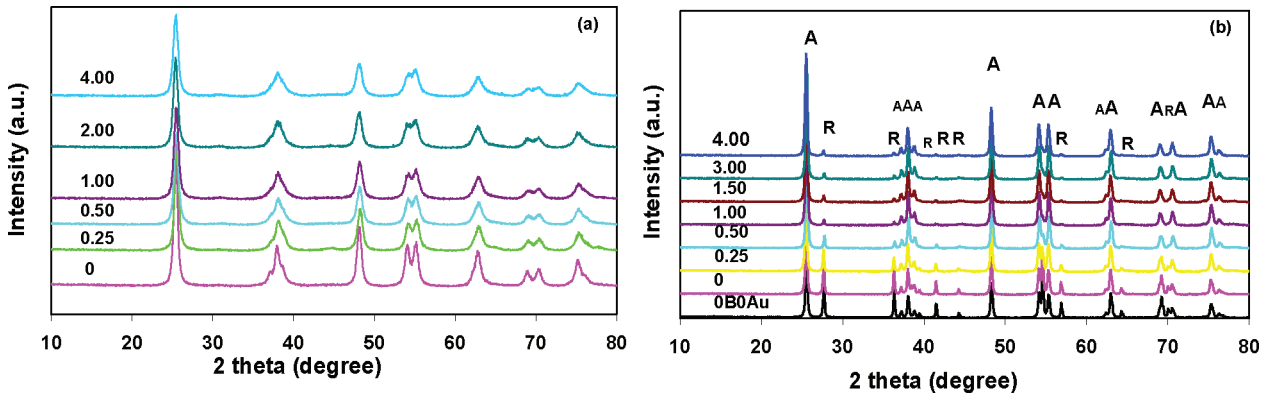

Figure 3. X-ray diffraction patterns of (a) the $Au/B/TiO_2$ composites with 0−4 wt % B and 2 wt % Au initial content, calcined at 450 °C, and (b) the pure TiO_2 control (0B0Au) and $Au/B/TiO_2$ composites with 0−4 wt % B and 2 wt % Au initial content calcined at 650 °C. (A = anatase and R = rutile).

dx.doi.org/10.1021/am201695c | ACS Appl. Mater. Interfaces 2012, 4, 476−482

boron concentration during synthesis increased (Figure 5). The gold content (not shown) was relatively constant across the

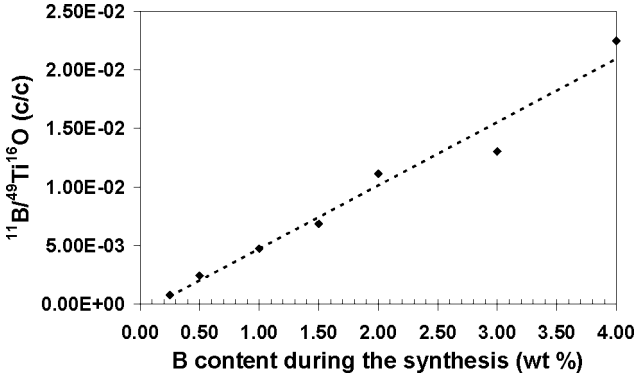

Figure 5. Ratio of the B/TiO (counts/counts) in the Au/B/TiO_2 composites determined by secondary ion mass spectrometry for various boron contents during the synthesis (the average raster rate was 0.0016 μm s^{-1} and the sputter time was generally 3000 s). The Au content was 2 wt % during the synthesis.

samples with different boron content, indicating that the amount of boron in the sample had minimal influence on the gold incorporation.

Photoluminescence (PL) is a highly sensitive technique used to investigate the photophysical and photochemical properties of solid semiconductors, and can provide information on charge separation/recombination of photoinduced charged carriers (electron/hole), as well as surface defects.[33−35] PL emission mainly results from the recombination of excited electrons/holes, where a lower PL intensity indicates a lower recombination rate of excited electrons/holes.[36] There are two types of PL phenomenon: the band−band PL and the excitonic PL, as determined by their attributes and formation mechanism.[37] The peaks located around 397 and 426 nm are mainly ascribed to the emission of the band gap transition.[37,38] In addition, the other peak at around 490 nm was attributed to the excitonic PL, which mainly resulted from surface oxygen vacancies and defects of the Au/B/TiO_2 network.[37,38] The B/TiO_2 samples have a higher PL intensity compared to Au/B/TiO_2 samples, Figure 6, thus demonstrating that the addition of gold nanoparticles effectively suppressed the charge recombination. For the composites calcined at 450 °C, the PL intensity (Figure 6a) increased with increased boron doping, which maybe a result of surface defects introduced by boron doping, and therefore more charge trapping leading to increased charge recombination. With gold nanoparticles present, the effect of B doping on the PL intensity was limited. For the samples calcined at 650 °C (Figure 6b), the addition of gold also decreased the PL intensity; however, the boron doping had little effect.

The blue color of the samples after calcination also indicated the incorporation of gold nanoparticles in the TiO_2 network. UV−vis diffuse reflectance spectra of the calcined samples showed a marked decrease of reflectance in the visible wavelength at around 580 nm due to the plasmon resonance of gold. The intensity of the reflectance remained similar for all of the Au/B/TiO_2 samples regardless of the boron content, indicating a similar gold content and size within the samples (see Figure S2 in the Supporting Information).

TiO_2 is an indirect band gap semiconductor,[39,40] and therefore the band gaps of the samples (see Table S1 in the

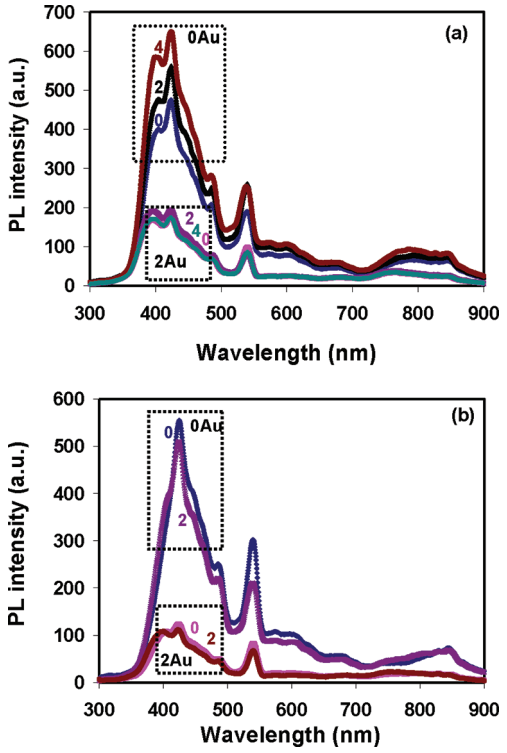

Figure 6. Photoluminescence spectra of B/TiO_2 samples with 0, 2, and 4 wt % boron (large box) and Au/B/TiO_2 composites with 2 wt % Au and 0, 2, or 4 wt % boron (small box), calcined at (a) 450 °C and (b) 650 °C.

Supporting Information) were estimated using the indirect mode (for details, see the Supporting Information, Figure S3). For all the boron doped materials, the optical absorption from the gold nanoparticles were similar since the gold nanoparticle properties remained the same in all cases (e.g., gold particle diameter and loading amount). When the samples were calcined at 450 °C, the titania band gap decreased from 3.16 ± 0.05 eV in the control sample to 2.89 ± 0.05 eV for the boron doped TiO_2. Therefore, the light absorption threshold extended from 387 nm to visible light, around 430 nm. It was noted that varying the quantity of boron during synthesis barely (450 °C) or slightly (650 °C) altered the band gap. For example, when the samples were calcined at 650 °C, the band gap of nondoped titania was 2.76 ± 0.05 eV; but with the addition of boron at 0.25 wt %, the band gap increased to 2.87 ± 0.05 eV. As the boron amount was increased further, the band gap increased gradually to 2.95 ± 0.05 eV with 4 wt % boron doping. The increase in band gap was mainly due to the presence of boron suppressing the rutile phase formation, the rutile phase having a lower band gap of 3.0 eV. The change in crystal phase of the titania also induced different band gaps in samples calcined at 450 and 650 °C. After calcination at 450 °C, the anatase phase (with a band gap of 3.2 eV) was obtained, however after calcination at 650 °C, the rutile crystal phase was also present (with a band gap of 3.0 eV). The origin of the absorption band in the visible range for non-metal-doped TiO_2 is debatable.[17] There are a number of explanations: (i) introduction of the localized state in the band gap,[41] (ii) intrinsic defects, including oxygen vacancies,[42] (iii) formation of oxygen vacancies and the advent of color centers to absorb visible light,[43] and (iv) reduction of Ti^{4+} to Ti^{3+} by oxygen as a result of B doping in the interstitial position.[44] With the aid of

dx.doi.org/10.1021/am201695c | ACS Appl. Mater. Interfaces 2012, 4, 476−482

the theoretical calculation, it was reported that boron doping has two types of interstitial species, pseudotetrahedral-coordinated Q* and tricoordinated T*.[14] The Q* unit tends to promote visible light absorption.[14] We assumed in our system that oxygen vacancies and substitutional B contributed to the visible-light absorption and band-gap reduction.

Photocatalytic Activity of Au/B/TiO_2. The photocatalytic (PC) activity of the samples was investigated by monitoring changes in methylene blue (MB) concentration under visible light irradiation (Figure 7). The concentration decrease of

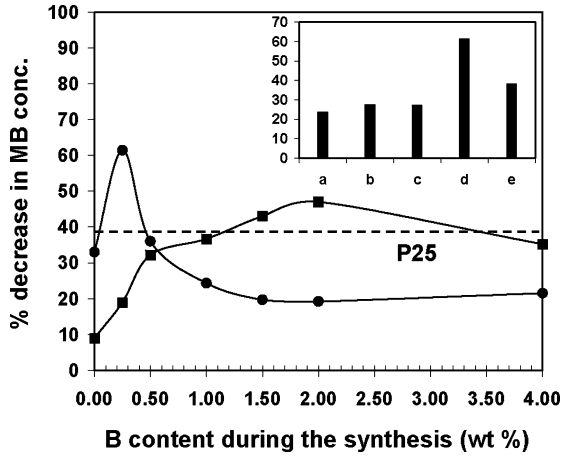

Figure 7. Photocatalytic efficiency of the Au/B/TiO_2 composites after 120 min visible light irradiation as a function of initial boron content at different calcination temperatures: 450 °C (square) and 650 °C (circle). The inset shows PC activity of (a) TiO_2 control, (b) 2 wt % Au/TiO_2, (c) 0.25 wt % B/TiO_2, (d) Au/B/TiO_2 composite with 2 wt % Au and 0.25 wt % boron, calcined at 650 °C, and (e) commercial Degussa P25 titania.

methylene blue without any photocatalyst present was below 3%. Before monitoring the PC reaction, the photocatalysts were placed in MB solution in the dark to reach absorption equilibrium. The initial concentration (C_0) was the same for all samples. The PC activity of the samples calcined at 450 °C increased steadily as the boron content increased. It reached a maximum degradation of 48% when the boron content was 2.0 wt %, which was almost five times higher than the nondoped Au/TiO_2 sample. When the samples were calcined at 650 °C, the introduction of boron significantly enhanced the PC activity to 62% at a low initial content of 0.25 wt %. This was double that of the pristine titania sample and ca. 50% higher than the commercial Degussa P25 titania (39%). When the boron amount was further increased, the PC activity decreased. The inset in Figure 7 highlights the enhancement of doping with boron and incorporating gold nanoparticles. Both the 0.25 wt % B/TiO_2 sample without Au and the 2 wt % Au/TiO_2 sample without boron, calcined at 650 °C, were photoactive under visible light. When combined together, the degradation was double that of either the boron doped or gold deposited reference samples (both slightly higher than the control titania sample), and markedly greater than commercial Degussa P25 titania.

PC activity is simultaneously influenced by boron doping and gold deposition. Boron doping can effectively retard the crystal growth of anatase (450 °C) and phase transition from anatase to rutile (650 °C) and modify the band gap to allow visible light absorption. The optimum boron content for photocatalysis was dependent on the calcination temperature. Better PC activity occurs when the materials are well crystallized,[45] with larger cystals having longer distances for electron and hole migration, which then decreases recombination compared to smaller crystals.[46] With the pure anatase phase samples (450 °C) at a high level of boron doping (e.g., 4 wt % boron), anatase phase growth was suppressed significantly leading to a lower crystallinity, and hence a decrease in PC activity.

With the mixed phase samples (650 °C), the addition of boron can alter the phase composition ratio, which influenced the photocatalytic performance. Other researchers have also found the same phenomena for mixed phase titania.[47,48] The contact between the anatase and rutile crystals benefits the electron transfer, and the commercial product Degussa P25 titania (benchmark photocatalyst) has an anatase molar ratio of 0.78. The highest PC activity in this study was achieved at a similar anatase molar fraction of 0.76. The enhancement in photocatalytic activity of TiO_2 after Au deposition under visible light was possibly due to the sensitization of TiO_2 as a result of gold surface plasmon excitation.[49] Moreover, the gold nanoparticles serve as an electron sink as demonstrated by the decreased PL intensity in the presence of gold, which implies a decreased recombination rate of the electrons and holes,[50] and further increases the PC activity of the boron-doped TiO_2.

CONCLUSIONS

This study has shown a simple approach to the preparation of a visible light responsive photocatalyst through the combination of boron doping and gold nanoparticle incorporation in porous titania materials templated by using an agarose gel. The maximum PC activity (48% for 2.0 wt % boron in samples calcined at 450 °C and 62% for 0.25 wt % boron in samples calcined at 650 °C) was achieved by tuning the band gap, the crystallinity, and the ratio of anatase to rutile. The PC activity was also improved by decreased electron/hole recombination using gold nanoparticles as electron sinks. This method is versatile and could be used in an extended study of boron doping in combination with the incorporation of other noble metal nanoparticles for improving activity in the visible range.

ASSOCIATED CONTENT

Supporting Information

Characterization of pore size distribution, diffuse UV−vis, band gap calculation, table of crystal size, band gap, anatase to rutile ratio. This material is available free of charge via the Internet at the http://pubs.acs.org.

AUTHOR INFORMATION

Corresponding Author

*E-mail: rcaruso@unimelb.edu.au. Fax: 61 3 9347 5180. Tel: 61 3 8344 7146.

ACKNOWLEDGMENTS

This research was financially supported by the Australian Research Council's Discovery Project Scheme (DP0344565) and an award (AINGRA08083) from the Australian Institute of Nuclear Science and Engineering. R.A.C. acknowledges the Australian Research Council for a Future Fellowship (FT0990583). Mr. T. Dornom, Mr. A. J. Atanacio, Dr. D. R. G. Mitchell, and Dr. S. Crawford are acknowledged for participation in photocatalysis analysis, SIMS analysis, TEM analysis and ultramicrotoming samples, respectively. Ms. M.

Chee Kimling and Mr. W. A. McMaster are appreciated for the helpful discussions regarding DTA data analysis.

REFERENCES

(1) Linsebigler, A. L.; Lu, G. Q.; Yates, J. T. *Chem. Rev.* **1995**, *95*, 735.
(2) Stafford, U.; Gray, K. A.; Kamat, P. V. *Heterog. Chem. Rev.* **1996**, *3*, 77.
(3) Mo, S. D.; Ching, W. Y. *Phys. Rev. B* **1995**, *51*, 13023.
(4) Wang, X. D.; Caruso, R. A. *J. Mater. Chem.* **2011**, *21*, 20.
(5) Hoffmann, M. R.; Martin, S. T.; Choi, W. Y.; Bahnemann, D. W. *Chem. Rev.* **1995**, *95*, 69.
(6) Chen, X.; Mao, S. S. *Chem. Rev.* **2007**, *107*, 2891.
(7) Yu, J. C.; Ho, W. K.; Yu, J. G.; Yip, H.; Wong, P. K.; Zhao, J. C. *Environ. Sci. Technol.* **2005**, *39*, 1175.
(8) In, S.; Orlov, A.; Berg, R.; Garcia, F.; Pedrosa-Jimenez, S.; Tikhov, M. S.; Wright, D. S.; Lambert, R. M. *J. Am. Chem. Soc.* **2007**, *129*, 13790.
(9) Grey, I. E.; Li, C.; MacRae, D. M.; Bursill, L. A. *J. Solid State Chem.* **1996**, *127*, 240.
(10) Moon, S. C.; Mametsuka, H.; Tabata, S.; Suzuki, E. *Catal. Today* **2000**, *58*, 125.
(11) Chen, D.; Yang, D.; Wang, Q.; Jiang, Z. Y. *Ind. Eng. Chem. Res.* **2006**, *45*, 4110.
(12) Zhao, W.; Ma, W. H.; Chen, C. C.; Zhao, J. C.; Shuai, Z. G. *J. Am. Chem. Soc.* **2004**, *126*, 4782.
(13) Liu, G.; Zhao, Y.; Sun, C.; Li, F.; Lu, G. Q.; Cheng, H.-M. *Angew. Chem., Int. Ed.* **2008**, *47*, 4516.
(14) Feng, N.; Zheng, A.; Wang, Q.; Ren, P.; Gao, X.; Liu, S.-B.; Shen, Z.; Chen, T.; Deng, F. *J. Phys. Chem. C* **2011**, *115*, 2709.
(15) Liu, G.; Sun, C. H.; Cheng, L. N.; Jin, Y. G.; Lu, H. F.; Wang, L. Z.; Smith, S. C.; Lu, G. Q.; Cheng, H. M. *J. Phys. Chem. C* **2009**, *113*, 12317.
(16) Klauson, D.; Portjanskaya, E.; Budarnaja, O.; Krichevskaya, M.; Preis, S. *Catal. Commun.* **2010**, *11*, 715.
(17) Wu, Y.; Xing, M.; Zhang, J. *J. Hazard. Mater.* **2011**, *192*, 368.
(18) Jakob, M.; Levanon, H.; Kamat, P. V. *Nano Lett.* **2003**, *3*, 353.
(19) Ismail, A. A.; Bahnemann, D. W. *J. Adv. Oxid. Technol.* **2009**, *12*, 9.
(20) Dozzi, M. V.; Prati, L.; Canton, P.; Selli, E. *Phys. Chem. Chem. Phys.* **2009**, *11*, 7171.
(21) Chiarello, G. L.; Forni, L.; Selli, E. *Catal. Today* **2009**, *144*, 69.
(22) Primo, A.; Corma, A.; Garcia, H. *Phys. Chem. Chem. Phys.* **2011**, *13*, 886.
(23) Li, H.; Bian, Z.; Zhu, J.; Huo, Y.; Li, H.; Lu, Y. *J. Am. Chem. Soc.* **2007**, *129*, 4538.
(24) Bannat, I.; Wessels, K.; Oekermann, T.; Rathousky, J.; Bahnemann, D.; Wark, M. *Chem. Mater.* **2009**, *21*, 1645.
(25) Wang, X. D.; Mitchell, D. R. G.; Prince, K.; Atanacio, A. J.; Caruso, R. A. *Chem. Mater.* **2008**, *20*, 3917.
(26) Zhou, J. F.; Zhou, M. F.; Caruso, R. A. *Langmuir* **2006**, *22*, 3332.
(27) Wang, X. D.; Egan, C. E.; Zhou, M. F.; Prince, K.; Mitchell, D. R. G.; Caruso, R. A. *Chem. Commun.* **2007**, 3060.
(28) Toyoda, M.; Nanbu, Y.; Nakazawa, Y.; Hirano, M.; Inagaki, M. *Appl. Catal., B: Environ.* **2004**, *49*, 227.
(29) Akpan, U. G.; Hameed, B. H. *J. Hazard. Mater.* **2009**, *170*, 520.
(30) Arbiol, J.; Cerda, J.; Dezanneau, G.; Cirera, A.; Peiro, F.; Cornet, A.; Morante, J. R. *J. Appl. Phys.* **2002**, *92*, 853.
(31) Spurr, R. A.; Myers, H. *Anal. Chem.* **1957**, *29*, 760.
(32) Smith, S. J.; Stevens, R.; Liu, S. F.; Li, G. S.; Navrotsky, A.; Boerio-Goates, J.; Woodfield, B. F. *Am. Mineral.* **2009**, *94*, 236.
(33) Shi, J. Y.; Chen, J.; Feng, Z. C.; Chen, T.; Lian, Y. X.; Wang, X. L.; Li, C. *J. Phys. Chem. C* **2007**, *111*, 693.
(34) Abazovic, N. D.; Comor, M. I.; Dramicanin, M. D.; Jovanovic, D. J.; Ahrenkiel, S. P.; Nedeljkovic, J. M. *J. Phys. Chem. B* **2006**, *110*, 25366.
(35) Nakajima, H.; Mori, T.; Shen, Q.; Toyoda, T. *Chem. Phys. Lett.* **2005**, *409*, 81.
(36) Li, X. Z.; Li, F. B. *Environ. Sci. Technol.* **2001**, *35*, 2381.
(37) Yu, J.; Yue, L.; Liu, S.; Huang, B.; Zhang, X. *J. Colloid Interface Sci.* **2009**, *334*, 58.
(38) Li, X.; Goring, P.; Pippel, E.; Steinhart, M.; Kim, D. H.; Knoll, W. *Macromol. Rapid Commun.* **2005**, *26*, 1173.
(39) Irie, H.; Watanabe, Y.; Hashimoto, K. *J. Phys. Chem. B* **2003**, *107*, 5483.
(40) Wu, P. G.; Ma, C. H.; Shang, J. K. *Appl. Phys. A: Mater. Sci. Process.* **2005**, *81*, 1411.
(41) Chen, X.; Burda, C. *J. Am. Chem. Soc.* **2008**, *130*, 5018.
(42) Serpone, N. *J. Phys. Chem. B* **2006**, *110*, 24287.
(43) Kuznetsov, V. N.; Serpone, N. *J. Phys. Chem. C* **2009**, *113*, 15110.
(44) Gopal, N. O.; Lo, H.-H.; Ke, S.-C. *J. Am. Chem. Soc.* **2008**, *130*, 2760.
(45) Ma, B.; Goh, G. K. L.; Ma, J. *J. Electroceram.* **2006**, *16*, 441.
(46) Tanaka, K.; Capule, M. F. V.; Hisanaga, T. *Chem. Phys. Lett.* **1991**, *187*, 73.
(47) Bojinova, A.; Kralchevska, R.; Poulios, I.; Dushkin, C. *Mater. Chem. Phys.* **2007**, *106*, 187.
(48) Kim, S.; Ehrman, S. H. *J. Colloid Interface Sci.* **2009**, *338*, 304.
(49) Kowalska, E.; Mahaney, O. O. P.; Abe, R.; Ohtani, B. *Phys. Chem. Chem. Phys.* **2010**, *12*, 2344.
(50) Subramanian, V.; Wolf, E. E.; Kamat, P. V. *J. Am. Chem. Soc.* **2004**, *126*, 4943.